Preservation of AVO after Migration

Oliver Lahr and Gary F. Margrave

ABSTRACT

Choice of migration algorithms and seismic acquisition techniques are two contributing factors of how well Amplitude Variation with Offset (AVO) data is preserved. In this report, these effects are investigated using synthetic Shots and Common Offset Vectors (COV gathers), the latter being the 3D extension of Common Shot gathers. The data, both shots and gathers, were created from a 2D synthetic data set that is comprised of the three different AVO classes occurring at different horizontal layers, and was in turn created using elastic modeling. A simple orthogonal survey was used, with different data sets being created by varying the shot and receiver line spacing to simulate different levels of decimation. To mitigate the effect of these decimations and its associated seismic acquisition footprint, they were then migrated using Kirchhoff migration. It is the purpose of this report to show how well the Zoeppritz plot of the AVO anomalies pictured below could be reproduced for the input data shown in the well logs and associated table below, and identify the scenarios that one or the other migration techniques undertaken here.

INTRODUCTION

Since Mosher et. al. (1996) pointed out the benefits of migration before AVO analysis, numerous studies have been done to highlight the various factors effecting the preservation of seismic amplitudes. (Zhang and Brown (2001) summarized some of these, including the effect of using different acquisition geometries on amplitude preservation, the advantages of doing AVO studies in areas of shallower depths, the effect of anti-aliasing, caused by removing frequencies from the traces, on amplitude losses, and the effects of different types of migration on the preservation of amplitudes. Zheng et. al. (2010) further pointed out that incorrect migration weights and artifacts would also lead to a deterioration of amplitudes. Another factor, pointed out by SUnMsc, is that amplitude losses vary with reflector size as part of aperture and within the Fresnel zone during the migration.

On the other hand, according to Gespert (2002), there is obviously no substitution for proper acquisition in order to achieve true amplitudes to correct the original data. However, Downton, Holy et al (2010) have shown that acquisition footprint can be negated somewhat using 5D interpolation. Both studies also ask how different migration techniques, such as the well-known PSDM migration, pre-shot migration (Downton, 2010), and Common Offset Vector (COV) migration, will affect the preservation of amplitudes. In particular, COV migration uses Common Offset Vectors (Cary, 1999), which are in essence the 3D extension of 2D Common Offset Gathers. That is, COV gathers are created using Cartesian vectors based on the inline and xline components of a shot/receiver pair as compared to just the shot/receiver pair along a line in the 2D case. It should be noted that Gespert (2002) claims that PSDM migration is better than the COV(Common Offset Vector) migration, while Downton et. al. study concentrates mainly on pre-stack shot migration. This begs the question then of how pre-shot

migration quantitatively compares to COV migration. It is the purpose of this study to answer that question in light of various states of decimation of acquisition geometries. Before going on, it should also be pointed out that (Vermeer, 1998) developed the OVT(Overhead Vector Tile) gather method, which is very similar way to the COV method. This latter method will be described in more detail in the next section followed by the description of how the all the simulated data was created for this study. This will be followed by a brief description of the 3D Shot and 3D Common Offset migration algorithms. Some preliminary results of shot record migration at varying levels of decimation will then be shown, as well as some of the challenges that were met with the COV migrations will be pointed out. After that, future work will be addressed, followed by some concluding remarks. . Also, please note that this study is in essence a continuation of the work done by Cooper (2010).

AVO ANALYSIS – THEORY AND REVIEW

This section is meant to give a very brief overview of Amplitude Variation with Offset(AVO) and is by no means complete. However, this area has been studied extensively, with the following Yilmaz(2001), Feng and Bancroft (2006), Zhang and Brown (2001) and the Hampson-Russell software suite giving an excellent introduction and starting point for further research.

2.1 AVO – explained

The basic idea behind AVO theory is that reflection coefficients can be determined as a function of the incidence angle of a P-wave (Zoeppritz, 1919) travelling through the earth from some shot. This could be done by solving a set of equations. These equations, although correct, were overly complex, and have been simplified by a number of authors over the years, including Aki and Richards (2001) and Shuey (1985). These simplifications in turn have led to what we now know as Amplitude Variation with Offset theory, since the offset between the source and receiver pairs for a shot are directly related to the angle of incidence of the P-wave related to that shot. This has resulted in an improvement in the resolution of seismic images and has, among other things, greatly enhanced the detection of hydrocarbon reservoirs.

2.2 AVO Analysis: What has been done and what is recommended

In this regard, some excellent information summarizing what has been done in field of AVO analysis is given by Feng and Bancroft (2006). For instance, they point out why a correct processing sequence is paramount for good AVO analysis and underline the findings of Mosher et. al. (1996), that one of the main factors to ensure good AVO is to do a proper migration before the actual AVO analysis. That study in particular showed a marked improvement in the final AVO analysis after doing a wave-equation based migration as compared to no migration at all. Yilmaz (2007) repeated this experiment with the use of Common Reflection Surface gathers. We utilize Kirchhoff migration methods to repeat some of these findings, with a desire to qualitatively measure the success of this technique. We created our data in the following manner in order to carry out our investigation.

CREATION OF DATA SETS

The initial 2D synthetic seismic section was generated with Elastic Modeling and is discussed in Section 3.1 and 3.2. The creation of the shot gathers from this 2D data set is touched upon in Section 3.3, before some background on Common Offset Gathers and their generation is given in Section 3.4. Section 3.5 points some other studies related to the one undertaken here in order to highlight the validity of our research.

3.1 Elastic modeling

The data created here was done with the Reflectivity method developed by Kennett (1979). It involves calculating reflection and transmission coefficients at the different boundaries in a layered half-space, and has been found to give the best seismograms for modelling purposes (Mueller, 1985). The details of this method, although straight-forward, are beyond the scope of this report. They can, however, be found in the references mentioned above. The advantages of this method on the other hand have been aptly pointed out by Simmons and Backus (1994)..

3.2 The Data Set

In particular, the Hampson-Russell AVO modeling tool, was used to create our original 2D synthetic seismogram. We used a horizontal flat layered model that is illustrated in *Table 1* below. This data was taken from the CREWES report: " A review of AVO analysis (Hongbo, Zhang and R. James Brown, 2001", and is in fact originally from Rutherford & Williams, (1989). Note that the CREWES toolbox *reflectivity* code can also be used to generate the same data results based on the input described here.

Table 1. Layer parameters

Table 1. Layer Parameters.

Class	α_1/[m/s]	β_1/[m/s]	ρ_1/[kg/m^3]	α_2/[m/s]	β_2/[m/s]	ρ_2/[kg/m^3]
1	2000	879.88	2400	2933.33	1882.29	2000
2	2000	879.88	2400	2400	1540.05	2000
3	2000	879.88	2400	1963.64	1260.04	2000
4	2000	1000	2400	1598.77	654.32	2456.43

The visual representation of these logs is shown in *Figure 3.1*.

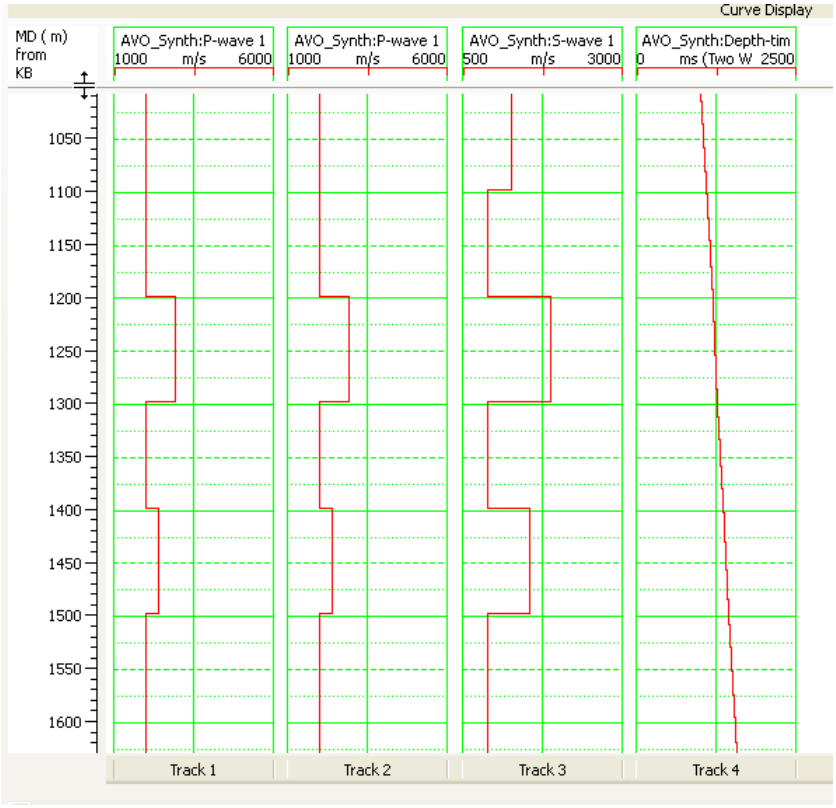

Figure 3.1: Logs used to create 2D seismogram using elastic modeling

The associated Zoeppritz curves of the data used here were displayed with CREWES MATLAB *zoepplot.m*. The P-wave amplitudes vs offsets and angles are shown in *Figure 3.3*. Note that at offset 500 m, the AVO 3 delta is -0.0158 and the AVO 1 anomaly is at -0.0217. This implies that the AVO 3 decreases at lesser rate than the AVO 1 anomaly, as expected.

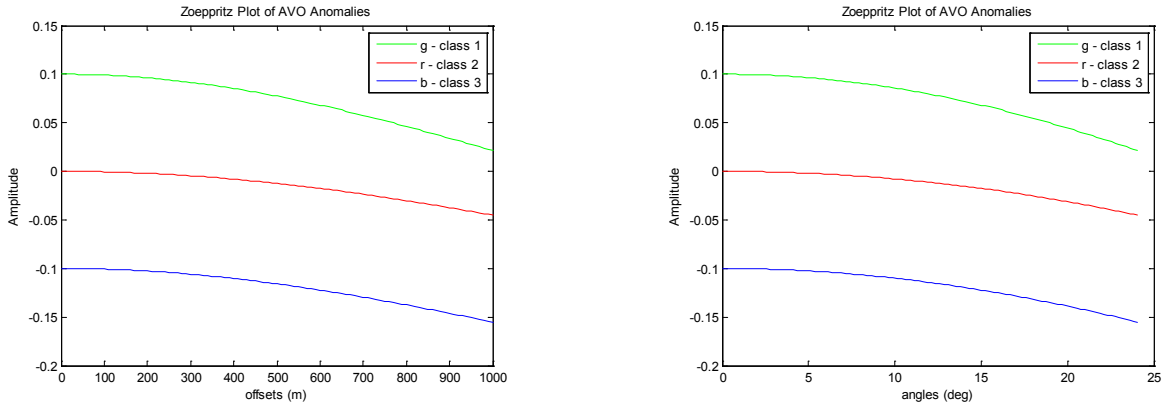

Figure 3.3: Amplitudes of P-P elastic waves vs offset and angle

That synthetic was then converted into a collection of 3D synthetic shot gathers, again using the CREWES matlab software. These were then migrated by shot record migration. The actual shot records were also resorted into the COV gathers, which were then migrated by 'common offset' migration. Both of these migration algorithms will be dealt with in the Section 4. The creation of the 3D data sets, on the other hand are described in more details in the next two subsections.

3.3 3D Shot Generation

To begin with, our 3D survey was assumed to be an orthogonal 1000 m by 1000 m area. Spacing of shot and receiver lines of 10m, 50m, 100 m, and 200 m were then used to create the increasingly decimated surveys for our experiments. Shots and receivers however, were kept constant at 10 m for all data sets.

The shot gathers were created by filling in the trace seen at a specific offset on the 2D synthetic section created in *Section 3.2* into the location of the receiver that was the length of that offset away from the shot of that particular shot record. Necessary adjustments were made when the offset in the 2D data set did not directly correspond to a particular shot – receiver offset in the shot gather.

In particular, if a shot was at x = 0, y = 0 and the receiver at x = 500, y = 500, the total offset would be sqrt(500^2+500^2) or 707.1068 m. This roughly corresponds to trace 707 of the 2D synthetic section. Utilizing a normal moveout correction technique, that trace was corrected to compensate for the 0.1068 m of the desired offset, and was then placed into the shot record at the corresponding location.

Results of this technique can be seen in the *Figures 3.4* to *3.6* on the next page. The shot locations of these gathers are at x = 0 m and y = 0 m, x = 500 m, y = 500 m and at x =1000m, y = 1000m. Notice that there are six events, corresponding to the AVO 3 anomaly coming in at ~1000 m, and going out at 1100 m., the AVO 1 anomaly going in at 1200 m and exiting at 1300 m, and the AVO 1 anomaly entering at 1400 m and leaving 1500 m.

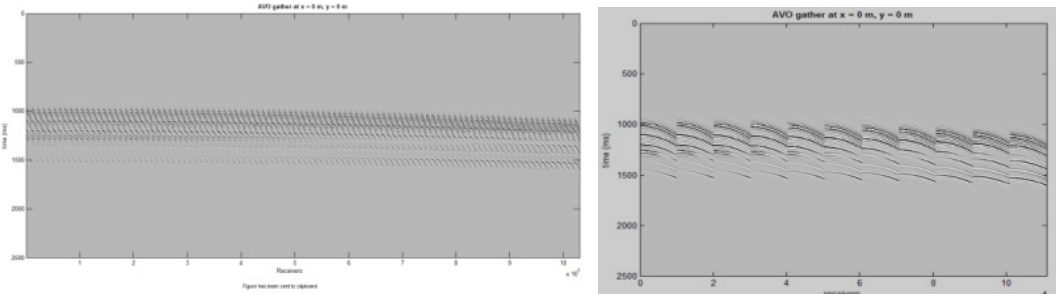

Figure 3.4: Shot gather 1, x = 0, y = 0, with all receivers shown on left, receiver line 1(y = 0) shown on right

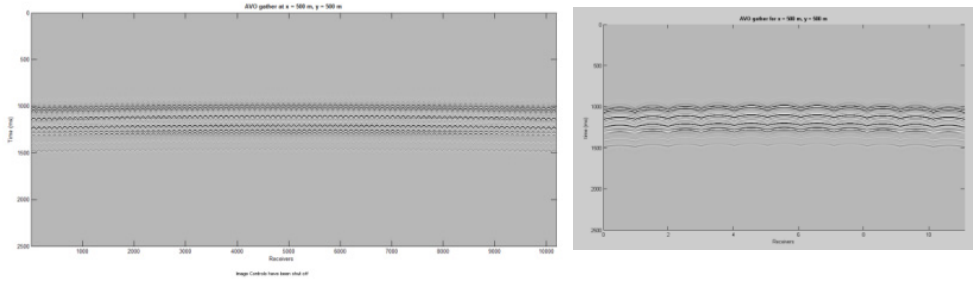

Figure 3.5: Shot gather 1, x = 500, y = 500, with all receivers shown on left, receiver line 6(y = 500 m) shown on right

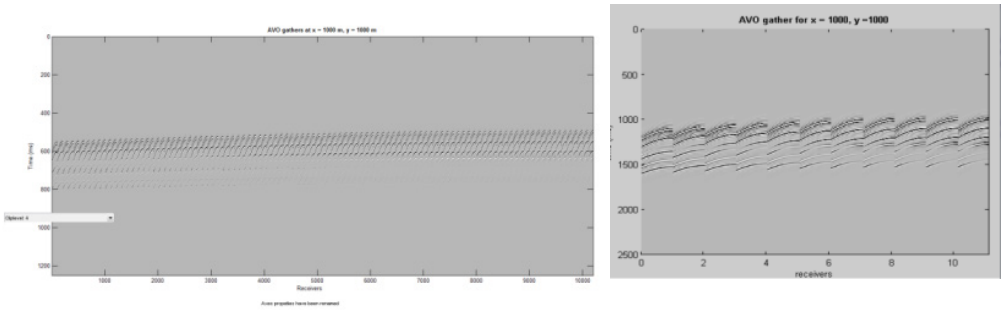

Figure 3.6: Shot gather 1, x = 1000, y = 1000, with all receivers shown on left, receiver line 6(y = 500 m) shown on right

3.4 Common Offset Vectors (COV)

Once the shot gathers were created, they were utilized to create the Common Offset Vector gathers. Before getting into the details of how this was done, the basic theory as presented by Cary (1999) and Vermeer (1998) is given, as well as the reasons for why they were created in this manner.

3.4.1. Common Offset Gathers and Vectors – 2D to 3D

To begin with, the idea behind Common Offset Gathers is shown in *Figure 3.4* below. As can be seen, offsets are measured from source to receiver, and these different offsets are denoted as multiples of h, where h is any measurement a user might choose, i.e. 10 m, 100 m, etc. For simplicities sake, shots are only shown here to progress in one direction.

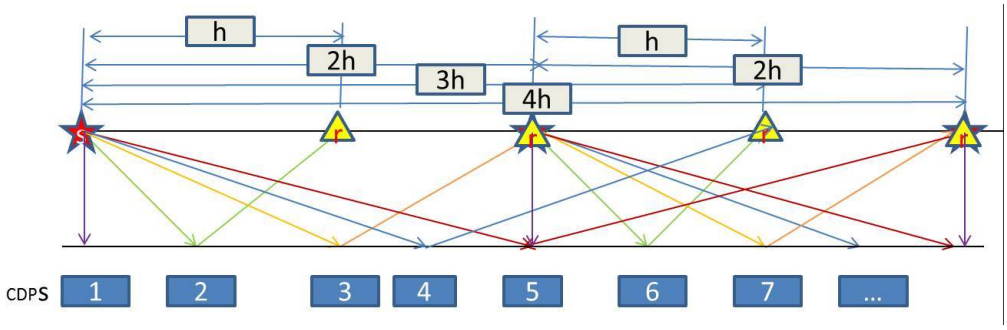

Figure 3.4 Illustration of Common Offset Gathers

The important point is that traces at common offsets from the shot can be collected into a gather. These then represent a stack, which in turn allow a user to better visualize that particular seismic section. An issue that can arise if the offsets are too large is aliasing, i.e. that not every midpoint in the survey is hit. This was pointed out by Cary (1999a). The solution is not to simply use the True Offset Gathers, specified by gathers corresponding to offsets h, 2h, etc., but to create Pseudo-Common Offset gathers in order to make sure every common mid-point in a grid (2D or 3D) is hit. This has led to a substantial reduction of aliasing after pre-stack migration and ensured clearer final images. In the case of this simple example, a Pseudo-Common Offset gather would consist of the offset traces at distance h, 2h, 3h, and 4h.

Cary (1999b) and Vermeer (1998) extend this concept to 3D. That is, they create COV gathers analogous to common offset gathers, with the COV bins being defined in terms of x and y coordinates.

According to Cary (1999) a COV tile or unit can be seen as shown in *Figure 3.5* and can be viewed as "…a selection of traces with common inline-offset and common crossline- offset (Cartesian coordinates), instead of common offset and azimuth (polar coordinates)."

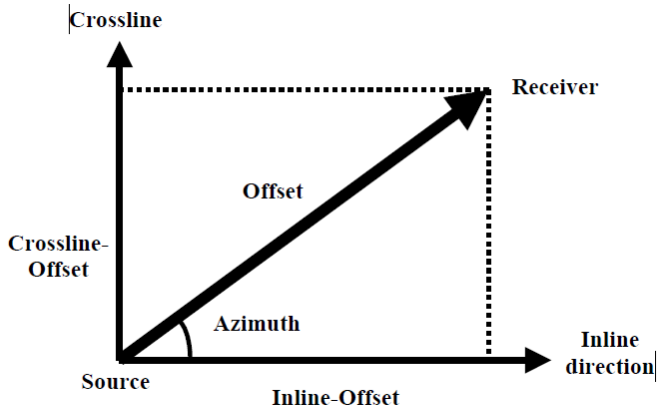

Figure 3.5: Illustration of a COV(Common Offset Vector) tile

The advantage of thinking of bins in this manner helps circumvent the issues involved in trying to organize 3D offsets in a manner of polar coordinates, as had been done up to that time. It also allows one to easily sort the gathers into 3D bins, due to the independence of the x and y axes.

The basic idea is that for each CMP, offset bins are created, where traces that fall within the range of that bin are averaged and then placed at the center of that bin. The bins are defined in exactly the same manner as for 2D (Cary 1999b), except now the y direction is taken into consideration. One immediate issue noted by Li (2008) is that one must compensate for large COVs as bins are calculated according to inline/xline fold(Cary 1999 and Li) and can yield sparse results. This also can lead to issues in calculating proper NMO values. This will be dealt with after the creation of COV gathers is dealt with.

3.4.2 Implementation of COVs

The first step for building COVs is to determine the bin size, and that this bin size be determined in regards to the patch chosen (Cordsen, 2000). An example of such a patch can be seen in *Figure 3.6* below. As shown, it is laid out in an orthogonal fashion, consisting of 11 receiver lines (blue) covering 1000 m with receivers (blue) spaced 10 m apart. There are also 11 shot lines covering 1000 m with shots(red) spaced 10 m apart.

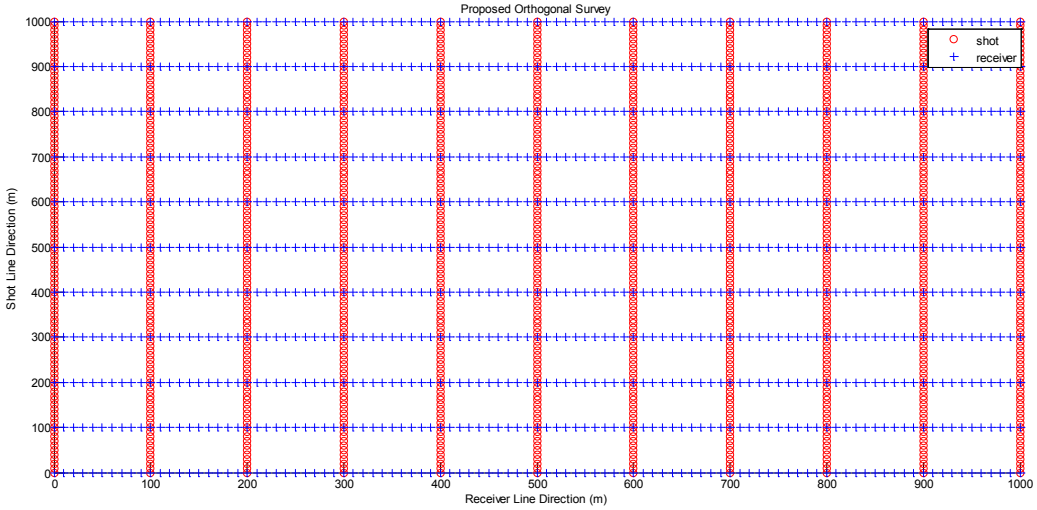

Figure 3.6: Orthogonal layout of shotlines(red) and receiver lines (blue) at 100 m each direction with shots and receivers 10 m apart

Utilizing this design, COV gathers can be constructed according to Cary (1999b) and Li (2008) by first calculating the entire fold of patch, i.e.

total fold = In-line fold times x-line fold *(3.1)*,

where the inline fold is defined to be the number of receivers times the receiver interval divided by 2 times the shot line interval, and the x-line fold is the number of receiver lines times 2.

For the survey shown above, the inline fold will be 100x11/(2*100) = 5 and the x-line fold is 11/2 = 5.5. The total fold will then be slightly more than 25.

Using these values, a COV gather for the example survey here can then be created by dividing the in-line patch length (1000 m) by the inline-fold (5.5) and the x-line patch length (1000 m) by x-line fold ,(5). This will yield bin sizes of ~200m x 200m or 200m x 200 m (Li, 2008).

3.4.3 Issues with implementation of COV gathers in this study

Now, according to Cary (1999b) and Li (2008), it is imperative that every CMP in the survey is hit, and that the bins not be too big, so not to end up with sparse data. Unfortunately, in light of the calculations for the example survey above, this is not the case. In fact, bin sizes of ~400mx400m would be needed to hit every cmp in the survey. Furthermore, a fold map using all shots and receivers indicate that a fold map (*Figure 3.7*) should be obtained, and that the maximum fold be 121. This definitely does not agree with the total fold calculated in the previous section. Finally, the non-integral value of fold calculated above is not recommended.

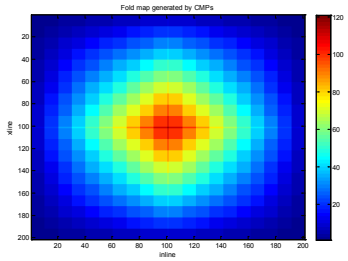

Figure 3.7 Fold map for current survey

To circumnavigate these issues, i.e. in order to hit every CMP in the survey, it is necessary to create bins of size 200m x 200m. This has in fact been done. However the

Table 3.1: Simulated layout of COV bins for this study with maximum offsets of 1000 and -1000, which guarantees the fold determined above.

-1000 - 1000	-800 – 1000	-600 - 1000	-400 - 1000	-200 – 1000	0 - 1000	200- 1000	400 - 1000	600 - 1000	800 - 1000	1000 – 1000
-1000 - 800	-800 – 800	-600 – 800	-400 – 800	-200 - 800	0 – 800	200- 800	400 – 800	600 - 800	800 – 800	1000 – 800
-1000 - 600	-800 - 600	-600 – 600	-400 – 600	-200 - 600	0 – 600	200- 600	400 - 600	600 - 600	800 - 600	1000 – 600
-1000 - 400	-800 - 400	-600 – 400	-400 – 400	-200 - 400	0 – 400	200- 400	400 - 400	600 - 400	800 - 400	1000 - 400
-1000 - 200	-800 - 200	-600 – 200	-400 – 200	-200 - 200	0 – 200	200- 200	400 - 200	600 - 200	800 - 200	1000 - 200
-1000 - 0	-800 - 0	-600 – 0	-400 – 0	-200 - 0	0 – 0	200- 0	400 – 0	600 - 0	800 – 0	1000 - 0
-1000 - -200	-800 - -200	-600 – -200	-400 - -200	-200 – -200	0 – -200	200 - -200	400 – -200	600 – -200	800 – -200	1000 – -200
-1000 - -400	-800 – -400	-600 – -400	-400 – -400	-200 – -400	0 – -400	200- -400	400 – -400	600 - -400	800 – -400	1000 – -400
-1000 - -600	-800 – -600	-600 – -600	-400 – -600	-200 – -600	0 – -600	200- -600	400 – -600	600 - -600	800 – -600	1000 – -600
-1000 - -800	-800 – -800	-600 – -800	-400 – -800	-200 – -800	0 – -800	200- -800	400 – -800	600 - -800	800 – -800	1000 – -800
-1000- -1000	-800 - -1000	-600 – -1000	-400 – -1000	-200 – -1000	0 - -1000	200- -1000	400 – -1000	600 – -1000	800 – -1000	1000 – -1000

maximum offset range in each direction will only be 500m instead of 1000m. But, this can be fixed by doubling the size of the patch in each direction. Hence, the survey is reset to include 22 receiver lines by 200 receivers. Now the

in-line fold = 200x11/2*100 = 11 *(3.2)* and the

x-line fold = 22/2 = 11 ***(3.3)*** resulting in a

total fold = 11 x 11 = 121 *(3.4)*

This desired fold result of 121 can be shown as per Figure 7 in (Li, 2008) and is illustrated in *Table 3.1*.

Furthermore, this is how we created the COV gathers for this study. As well, COV gathers with other line spacing of 10 m, 50 m and 200 m were calculated in a similar manner.

3.4.4 Testing of validity of COV volumes

As alluded to in *Section 3.4.1*, Common Offset Gathers, much like a stack, give a simple view of what the subsurface of a seismic survey looks like. COV gathers are no different in this regard. In particular, for this study we should see six visible, flat reflectors at the different event input times. These are at 0.996s, 1.098s, 1.198, 1.2268, 1.368 and 1.448 seconds. For instance, the first reflector, due to the AVO 3 anomaly starting, should thus be at 0.996 seconds, which corresponds to a depth of 1000m. The second reflector, due to the AVO 3 anomaly ending, should occur at 1.098 seconds, i.e. at about 1100 m, and so on. This is in fact the case for the results of the COV gather with zero offset shown in *Figure 3.8* here.

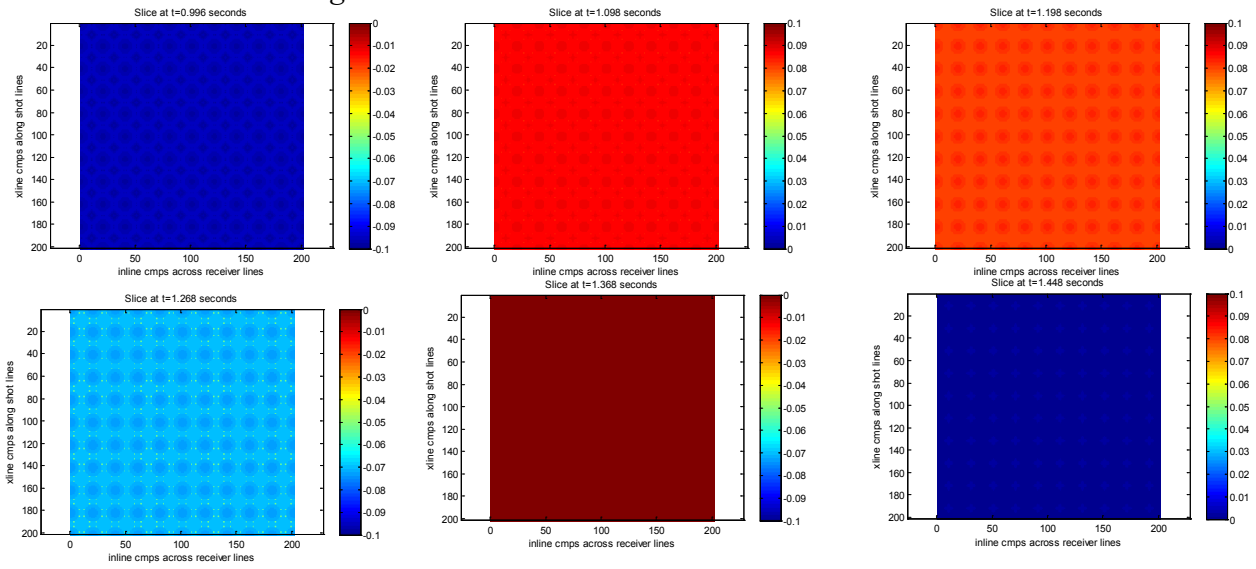

Figure 3.8: Top view of AVO for COV gather at 0 offset events. From top left to bottom right, by 2, AVO 3, AVO 0 and AVO 1(almost neglible, as expected)

Note that the amplitudes, indicated by the color bar on the right, have not been compensated for spherical spreading. Also note that as expected at 0 offset, the two lower depths are negligible as expected. The ringing that is seen in all of the slices can be explained by the non-zero offset traces adjacent to true zero offset traces

Another thing that needs to be considered is aperture. Obviously, for zero offset, one would expect the entire survey to be covered. This is in fact the case, as seen above. For non-zero offset, however, only a subset of survey should be seen. This is also the case, and is illustrated in *Figure 3.9*, which details the slices for a COV gathers with -600 m in the x and y directions.

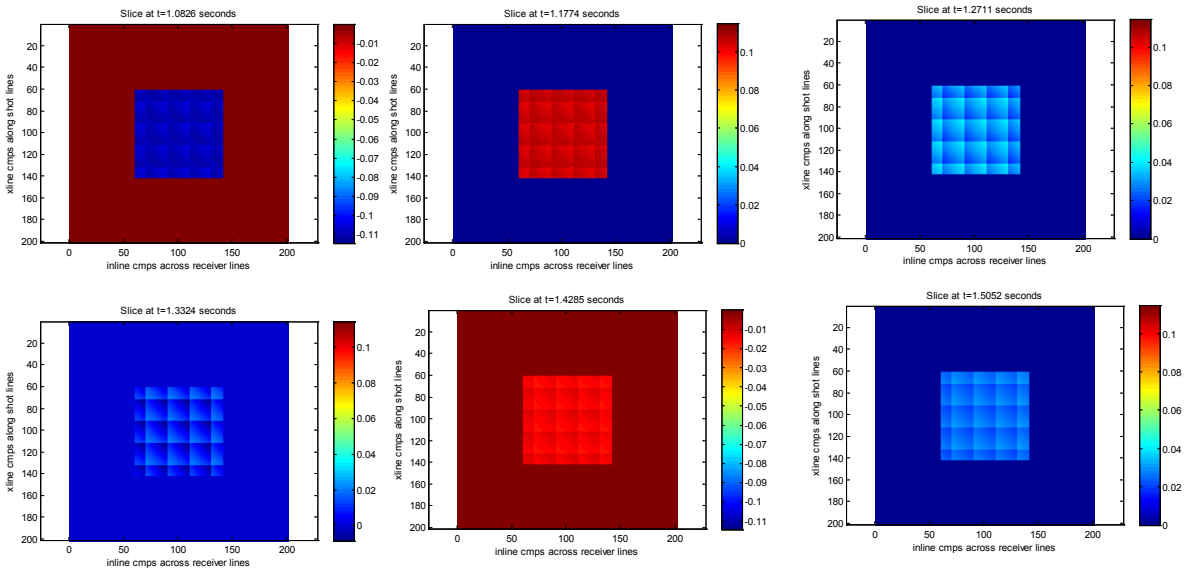

Figure 3.9: Top view of AVO for COV gather at -600m offset events. From top left to bottom right, by 2, AVO 3, AVO 0 and AVO 1(almost neglible, as expected)

Several other things to note here are the times are 'pushed' down, as expected, and that the AVO 2 events at 1.368 seconds (~1400m) and 1.448(~1500 m) have become visible. Also, the values for the AVO 1 event are now almost negligible.

The other 119 gathers of the expected 121 COV gathers for this survey, as well as all the gathers created for the other values of line spacing in this study, were validated in this manner.

3.4.5 Discussion of COV volume creation

As expected, the COV gathers each show the semblance of flat layers simulated from the original input well data. Due to normal moveout, as offset increases, the position of the layers can be found at lower depths. Also, symmetry will be preserved for our simple 3D dataset.. Another thing to note is that with an increase in offset, a lot of amplitude information at the bottom layers is lost.

3.4 Reasons for this study

A number of studies have been done to investigate the effects of migration and seismic acquisition on Amplitude preservation. For example, Gespert (2002) investigated the effects of acquisition on True Amplitudes and pointed out that PSDM migration yielded better than COV migration. He concluded that there is simply no substitute for proper acquisition. However, several studies utilizing 5D interpolation (Downton et. al.) have shown that improper seismic acquisition footprint can be negated to a certain degree. This implies that the entire problem has in fact been sidestepped. However, there still seems to

be no solid data to see how acquisition footprint relates to the preservation of amplitudes. It is the focus of this report to initiate this study.

MIGRATION OF DATA SETS

4.1 Kirchhoff Theory

In essence, Kirchhoff migration is an integral solution of the wave equation. It can be visualized in that it stores the results of the addition of amplitudes along a diffraction curve of an input record at the apex of that refraction. The original amplitudes are from the input data taken from a shot record or a Common Offset Vector, while the final result should represent an accurate image of the subsurface at that particular set of shot and receiver location. Here, we use shot records and COV gathers as our input, and migrate the data in the manner described. In particular, we deal with the migration of the shot gathers in *Section 4.2* and the migration of the COV gathers in *Section 4.3*. More detailed information on Kirchhoff migration can be found in (Yilmaz, 2001).

4.2 Migrating the shot data

The shot data in this study was migrated according to *Equation 5.2.23 (Bleistein et. al, 2001, p. 247)*, which has been implemented by the CREWES matlab code *kirkshot_3d.m*.

Figure 4.1 below shows the result of the migration of the AVO gather at shot x = 0, y =0, with

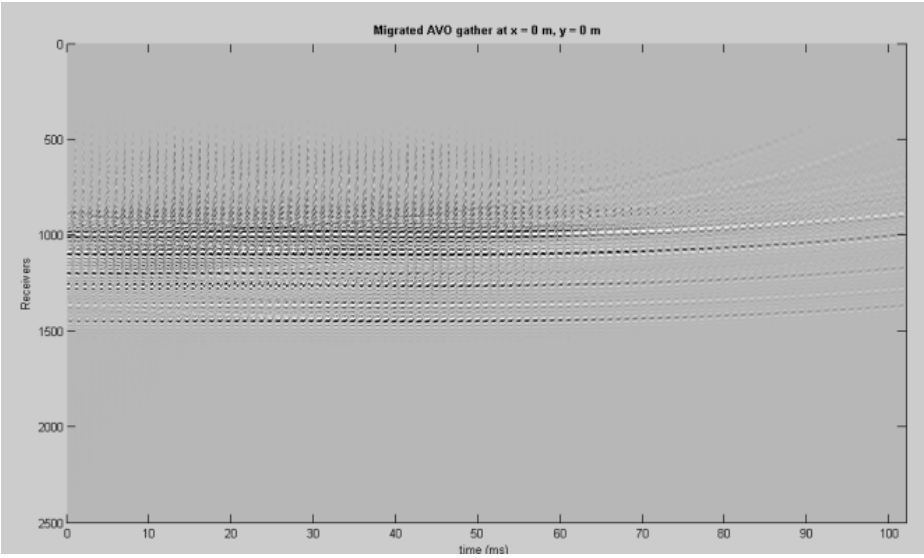

Figure 4.1: Migrated gather at shot located at x=0, y=0, side view

shot and receiver line spacing at 100 m, and all the receiver lines placed side by side. As expected, all the times have been corrected for, that is, the traces have all been shifted up to their expected positions. Also, the aperture of the migration is limited to half of the survey.

Figure 4.2 details the top view of the migration for that same. The slices can be seen at the expected times of the events, i.e. at 0.996, 1.098, 1.198 for the top row and 1.268 sec., 1.368 sec., 1.488 sec. for the bottom row. One can see the amplitudes decrease with increasing offset, that is the highest absolute value is seen for all maximum offsets, As expected, only half of the CMPs are covered, i.e. for the entire survey, only half of maximum shot-receiver distance. The amplitudes are in the line of the shot direction. In particular, they decrease, as expected for an AVO 3 anomaly, with increasing offset for Event 1 and increase with increasing offset for Event 2(when the AVO 3 anomaly is completed). There is symmetry at events 3 and 4, whose amplitudes correspond to the AVO 1 anomaly, and for the AVO 2 anomaly, the amplitudes start at 0. They decrease as expected for the event at 1.368 sec. and increase at 1.488 sec. Note that these values must still be accounted for scaling so that they better reflect the original values of this data.

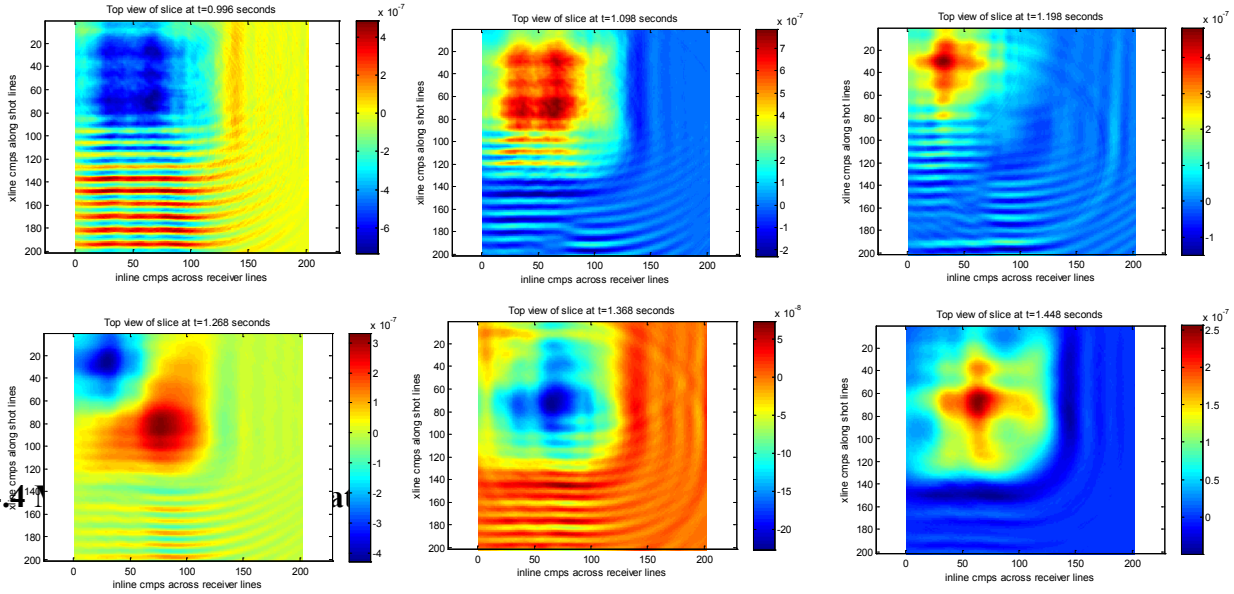

Figure 4.2 Top view of migrated shot x=0, y=0 gather, AVO 3 on top left, AVO 1 to AVO 2 on bottom right

The side views of the migrated AVO gather at shot x = 0, y =0 can be seen in *Figure 4.3*.

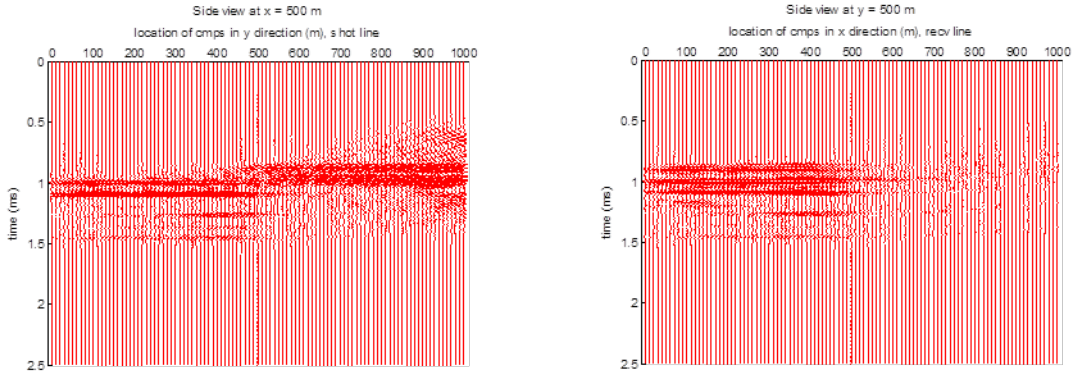

Figure 4.3: Side views of migrated shot gather at x=0, y=0

As expected, when y is constant, i.e. for the data along the shot line, the migrated data, with some migration smiles, goes up to maximum half offset or as far as the expected aperture pointed out previously. On the other hand, when x is constant, that is when the image is viewed along the constant shot line, the expected result is still within the aperture, but now the migration smiles are far more pronounced. This will need some investigation. However, for the amplitude analysis, they can be ignored.

The rest of the shot data can be displayed in a similar manner. For purposes of brevity, only the shot at x=500m, y=500m will be dealt with.

The view across all receivers is shown first in *Figure 4.4*. The aperture, as expected, is between 250 and 750 m, and the migration smiles are on each side of the aperture.

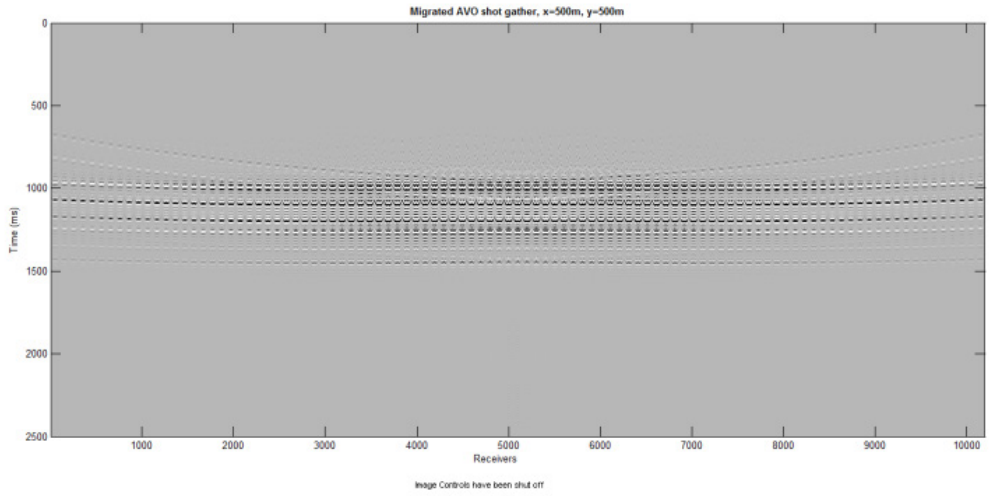

Figure 4.4: Migrated gather at shot located at x=500m, y=500m, side view

The top views of these migrated shot gathers are shown in *Figure 4.5*. One can see all the amplitudes decrease with increasing offset, before correcting themselves in a wave-like manner.

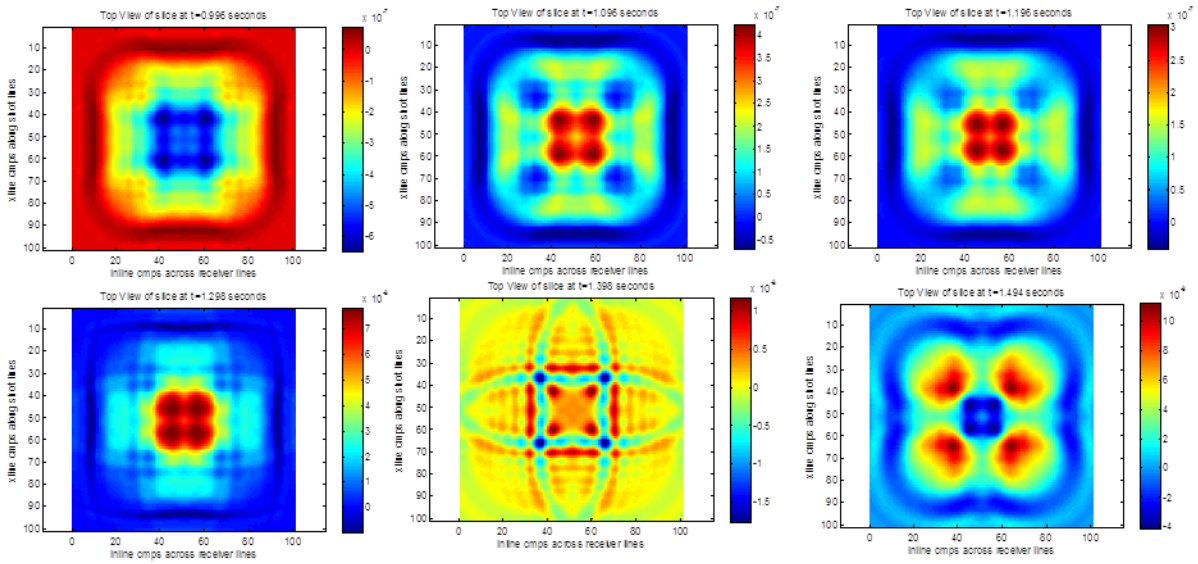

Figure 4.5: Top view of migrated shot x=500m, y=500m gather, AVO 3 on top left, AVO 1 to AVO 2 on bottom right

Also, only the center half of the CMPs are covered. In particular, for Event 1, amplitudes decrease starting from the shot location. These amplitudes are then inverted at Event 2, and as expected increased. This once again corresponds to the AVO 3 anomaly associated with the layer between these two events. The other four events can be discussed in a similar manner.

The side view is shown in *Figure 4.6*. Note that that both views now have 'clean' migrated data up to maximum half offset, i.e. expected CMP aperture, with some migration smiles.

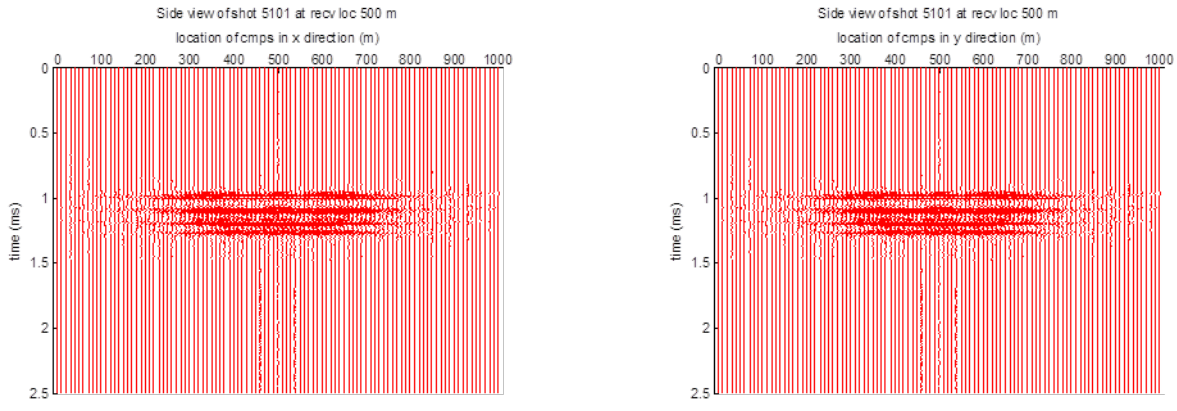

Figure 4.6: Side views of migrated shot gather at x=500m, y=500m

In summary, all migrated shot gathers are flat. The expected aperture covers only a quarter of all the common midpoints. There are the obvious migration smiles on the

edges, especially for shot 1, which will require further investigation. And as expected, all of the amplitudes generally decreased. This will be dealt with in more detail in *Section 5*.

4.4 Migrating the COV data

4.4.1 Common Offset Migration/Inversion

The Common offset vector migration algorithm was taken from (Bleistein, et. al, 2001, eq. 5.2.31, p. 249) and is a slight variation of the same procedure as was done for the Common-Shot Inversion. The algorithm was implemented by extending the existing CREWES *kirk_starckcos3d.m* code, which has been used for zero-offset migrations. We still

4.4.2 Results of Migrated COV gathers for survey with 100 m spacing

This section shows results of the migrations done on the orthogonal geometry with 100m line spacing.. The images shown here correspond directly to the original COV gathers shown in *Section 3.4.4*. To begin with, the COV gather with 0 offset in both the inline and xlind direction is shown first.

The top view of this set of migrated COV gathers is shown in *Figure 4*.7. The expected depths, as a result of the migration, are measured in meters, and are at ~ 998.2 m, 1098, 1198 as seen on the top row and at 1303 m, 1400 m, 1486 m on the bottom row. The amplitudes can be read from the color bar on the right of each migrated image. As expected, there the absolute amplitudes at the top and the bottom of an anomaly are essentially the same. As well, we can see that the amplitudes are more pronounced on the underlying grid.

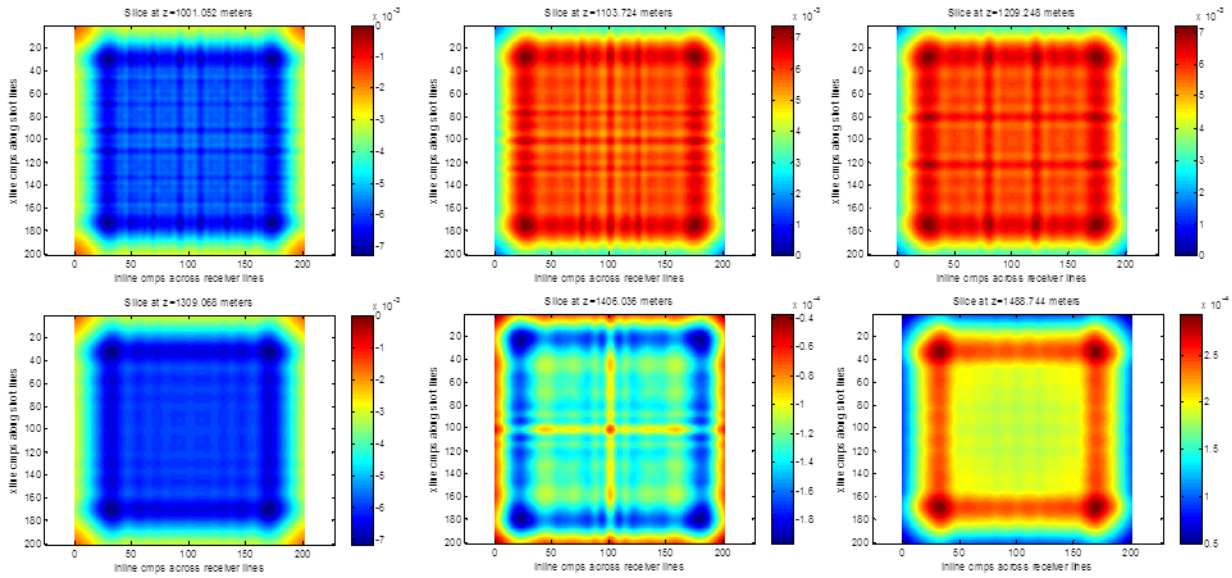

Figure 4.7: Top views of migrated COV gathers for zero offset, AVO 3 anomalies at 998.2 and 1098 m at top left, AVO1 anomalies at 1198 m and 1303 m, middle, and AVO 2 anomaly at 1400 m and 1486 m, bottom right

The second set of data illustrates the migrated data of COV gathers at -600 m in either direction. The same observations can be made as for the case of the zero-offset COV gathers. The migrated images are shown in *Figure 4.8*.

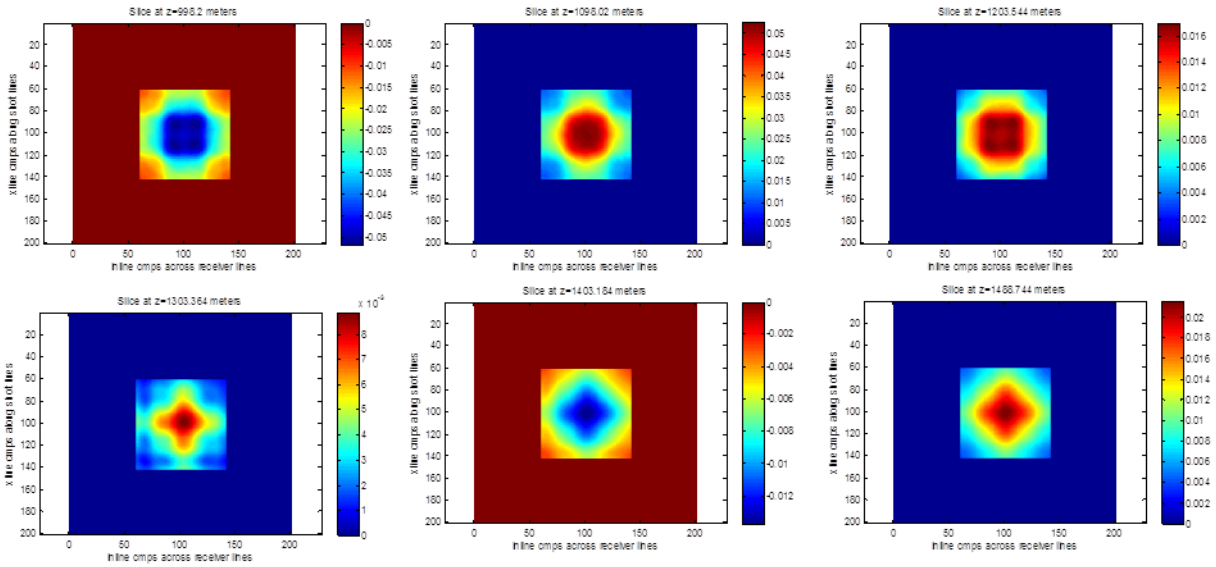

Figure 4.8: Top views of migrated COV gathers for offsets of -600 in either direction, AVO 3 anomalies at 998.2 and 1098 m at top left, AVO1 anomalies at 1198 m and 1303 m, middle, and AVO 2 anomaly at 1400 m and 1486 m, bottom right

4.4.4 Migration of COV volumes discussion

As expected, after migration, we get a semblance of flat layers for each gather. Also, after looking at other gathers with different offsets, we can see, as predicted, that all of the amplitudes seem to decrease with increasing offset.

To get a better handle on these results, the amplitudes need to be analyzed in regard to the different level of spacings, i.e. 10m, 50m, 100m and 100m, of the original data sets.

COMPARISON OF THE TYPES OF MIGRATION

Here, we look at all of results of the above migrations with respect to the different levels of spacing for the seismic array and see how well we can reproduce the Zoeppritz curves of each of the events of our study. In particular, *Section 5.*1will provide more details for the results of the shot record migration. *Section 5.2* will then deal with the COV gather migration.

5.1 Analysis of amplitudes for Shot Record Migration

In order to ‘recreate’ the Zoeppritz plots for each of the different surveys, we extracted all the amplitudes from the migrated data at the times we expected them to occur. So, for the 10 m survey, we looked for all the amplitudes at Event 1, when the AVO 3 anomaly occurs and stored them. We repeated this for the survey with 50 m, 100 m and 200 spacing. After adjusting for scaling using a least-squares approximation with the

theoretical Zoeppritz values, we plotted the 'adjusted' amplitudes against these theoretical values, knowing that the CMP locations and the shot locations could be used to determine the proper offset. The results are shown in *Figure 5.1*. The values for Event 1, for instance, can be seen at the top left corner of the figure.

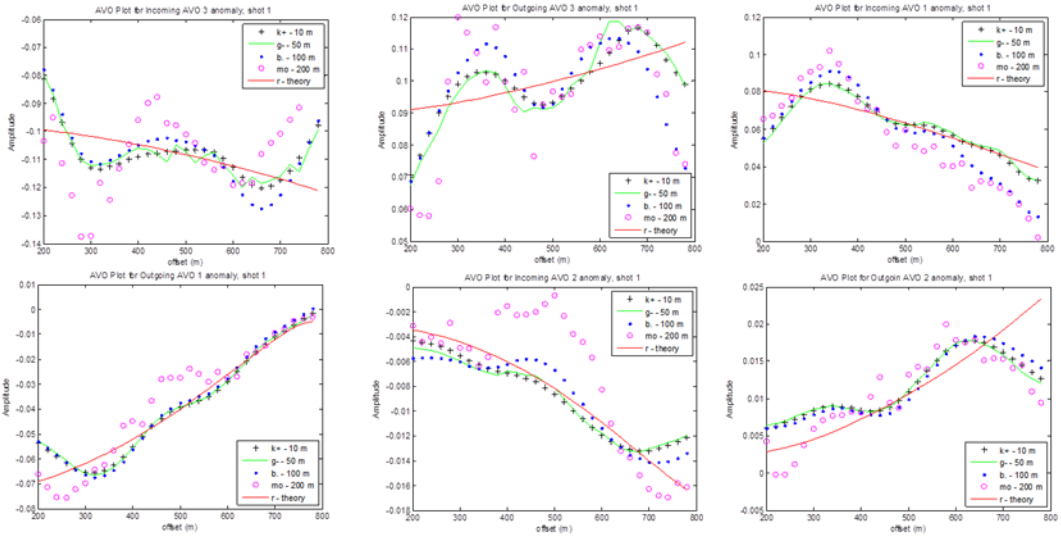

Figure 5.1: Shot 1 amplitudes of migrations for data with spacings of 10m, 50m, 100m and 200m compared to Zoeppritz curves for each event in experiment

As expected, the values for the 10 m spacing seem to best approximate the Zoeppritz curves for each event, while the values found for 200 m spacing are the worst. The area of interest was limited to the square denoted by the inline and xline locations of (200m,200m) and (800 m, 800 m). This was chosen after observing on *Figure 4.2* that data outside of this square led to poor fitting against the Zoeppritz curves. Obviously, a more rigorous calculation will be needed to confirm these results, as data points from all of the gathers, except the one for the 200 m line spacing, fitted the Zoeppritz curves almost 'equally' well.

Also note that these plots were generated for the first receiver line and shot 1. Plots for the other receiver lines led to similar conclusions. As well, an attempt to generate plots from data points in the entire gather yielded very poor results. This is currently also under investigation.

5.2 Analysis of amplitudes for COV Migration

On the other hand, attempts to properly match the Zoeppritz plots with the data of the COV migrations have not yet succeeded. The reasons for this shortcoming are currently being looked at. One should note that with an increase in line spacing, the number of data points will decrease substantially. Hence, for 200 m line spacing, we only have an insufficient number of data points, especially for line spacing of 200 m, where we will have six distinct data points for the entire survey. Since this also limits us to only being able to only use six data points of the other COV gathers, we are reasonable in assuming that our estimation of the 'actual' Zoeppritz curves will not be sufficient.

CONCLUSION AND FUTURE WORK

This report has served as a starting point to quantitatively determine how seismic data acquisition and different migration techniques affect amplitude preservation. We have seen some promising results for shot record migration, where, as expected, we have seen a deterioration of amplitudes values with an increase in line spacing. On the other hand, results of the COV migrations have been unsatisfactory. In this regard, we have come up with the insight that COV gathers created from surveys with larger line spacing might not yield enough data to properly preserve any initial amplitude values correctly.

ACKNOWLEDGEMENTS

We wish to thank everyone involved with the CREWES project for supporting this work.

REFERENCES

Aki, K. and P. G. Richards, 2002, Quantitative Seismology, Second Edition: University Science Books.

Bleistein, N., J. K. Cohen, and J. W. Stockwell, Jr., 2001, Mathematics of Multidimensional Seismic Imaging, Migration, and Inversion: Springer.

Cary, P. W., 1999a, Generalized sampling and "beyond Nyquist" imaging: CREWES Research Report, 11, 42.1-42.23.

Cary, P. W., 1999b, Common-offset-vector gathers: an alternative to cross-spreads for wide-azimuth 3-D surveys: 69th Annual International Meeting, SEG, Expanded Abstracts, 1496-1499.

Cooper, Joanna K., 2010, Seismic acquisition footprint: modelling and mitigation. M.Sc. Thesis, University of Calgary.

Cordsen, A., M. Galbraith, and J. Peirce, 2000, Planning Land 3-D Seismic Surveys: Society of Exploration Geophysicists.

Downton, J., 2010, Acquisition requirements for COV migration and azimuthal AVO, GeoCanada

Downton, J., Holy, D., Trad, D., Hunt, L., Reynolds, S., and Hadley, S., 2010, The effect of interpolation on imaging and azimuthal AVO: A Nordegg case study: 80th Annual International Meeting, SEG, Expanded Abstracts, 383-387.

Feng, Hong and Bancroft, John C., 2006, AVO principles, processing and inversion: CREWES Research Report, 18, 1-19.

Gesbert, S., 2002, From acquisition footprints to true amplitude: Geophysics, 67, 830-839.

Kennett, B., 1979, Theoretical reflection seismograms for elastic media: Geophysical Prospecting, Vol.27, p301-321.

Li. Xinxiang, 2008, An introduction to common offset vector trace gathering, CSEG Recorder, 33, No. 9, 28-34.

Mosher, C.C., Keho, T.H, Weglein A.B. & Foster, D.J., 1996, The impact of migration on AVO: Geophysics, 61, 1603-1615.

Mueller, G., 1985, The reflectivity method: a tutorial: J. Geophys., 58, 153–174.

Shuey, R.T., 1985. “A simplification of the Zoeppritz equations”, Geophysics, v.50, p. 609-614.

Simmons, J. L., and Backus, M., M., 1994, AVO modeling and the locally converted shear wave, Vol.59, p1237-1248.

Vermeer, G. J. O., 1998, 3-D symmetric sampling: Geophysics, 63, 1629-1647.

Yilmaz, O., 2001, Seismic Data Analysis, Society of Exploration Geophysicists.

Yilmaz, O., 2007, A unified 2D land seismic data analysis workflow, First Break, 25, 43-49.

Zhang, H and Brown R.J., 2001, A review of AVO analysis: CREWES Research Report, 13, 357-380.

Zheng, Y., Gray, S., CHEADLE, S. and Anderson, P., 2002, Factors Affecting AVO Analysis of Prestack Migrated Gathers: EAGE 64th Conference & Exhibition.

Zoeppritz, K., 1919, Erdbebenwellen VII. VIIb. Über Reflexion und Durchgang seismischer Wellen durch Unstetigkeitsflächen. Nachrichten von der Königlichen Gesellschaft der Wissenschaften zu Göttingen, Mathematisch-physikalische Klasse, 66-84.